the biophysical properties of the amino acids involved. For instance, in nine cluster transitions at least one charge change was involved, and substantial volume changes were involved in three transitions (table S5). The amino acid composition of the key positions seems limited by their exposed nature. Hydrophobic amino acids are typically located on the interior of a protein, where they can be shielded from solvent access. Tyrosine, which is only partially hydrophobic because of the hydroxyl group on its aromatic ring, was the only hydrophobic amino acid observed on the key positions. The necessity for maintaining a functional HA structure as well as escape from neutralizing antibodies may have restricted the range of possible amino acids.

The number of potential glycosylation sites on the A/H3N2 virus HA has steadily increased since 1968 (*19*), and the presence of carbohydrate side chains has been associated with shielding of antibody epitopes (*20*, *21*). A total of 14 HA positions are associated with glycosylation of the A/H3N2 viruses that circulated between 1968 and 2003. Two positions, 133 and 144, are located adjacent to the RBS. However, changes in glycosylation did not coincide with cluster transitions, and viruses belonging to the same antigenic cluster often had different glycosylation states (*22*). In agreement with these observations, the cluster-transition substitutions neither introduced nor deleted any glycosylation sites, and glycosylation was therefore not directly involved in the antigenic changes between the clusters. The location of the majority of the potential glycosylation sites away from the RBS could be the reason why changes in glycosylation have not played a major role in the antigenic change of A/H3N2 viruses.

To further expand these results, we examined the most recent antigenic cluster transitions in the other human seasonal influenza viruses: the B/Yamagata and B/Victoria lineages of the B viruses, and the pre-2009 A/H1N1 viruses (the current A/H1N1pdm09 viruses are yet to undergo a cluster transition). We found the same results as for the A/H3N2 viruses: The major antigenic change was caused by a single amino acid substitution in the corresponding region close to the RBS (Fig. 2C and figs. S11 to S13).

We find that although human A/H3N2 seasonal influenza viruses have fixed amino acid substitutions at 54 positions in antigenic sites, substitutions at only seven of these locations have been responsible for the major antigenic changes in these viruses to date. Moreover, these locations are all near the RBS of the HA, which suggests the mechanism for slowing the antigenic evolution of these viruses could be a reduction in receptor binding function. This small number of critical positions, and the restricted amino acid usage involved in antigenic cluster transitions, suggests that possibilities for important antigenic change of seasonal influenza viruses may be more restricted than previously thought, with potentially far-reaching consequences for understanding the underlying evolutionary mechanisms governing such viruses.

References and Notes

1. M. Akazawa, J. L. Sindelar, A. D. Paltiel, *Value Health* **6**, 107–115 (2003).
2. K. Stöhr, *Lancet Infect. Dis.* **2**, 517 (2002).
3. J. L. Virelizier, *J. Immunol.* **115**, 434–439 (1975).
4. J. Sui *et al.*, *Nat. Struct. Mol. Biol.* **16**, 265–273 (2009).
5. T. T. Wang *et al.*, *PLOS Pathog.* **6**, e1000796 (2010).
6. J. Steel *et al.*, *MBio* **1**, e00018-10 (2010).
7. D. C. Ekiert *et al.*, *Science* **333**, 843–850 (2011).
8. K. Koelle, S. Cobey, B. Grenfell, M. Pascual, *Science* **314**, 1898–1903 (2006).
9. S. E. Hensley *et al.*, *Science* **326**, 734–736 (2009).
10. W. M. Fitch, R. M. Bush, C. A. Bender, N. J. Cox, *Proc. Natl. Acad. Sci. U.S.A.* **94**, 7712–7718 (1997).
11. R. M. Bush, C. A. Bender, K. Subbarao, N. J. Cox, W. M. Fitch, *Science* **286**, 1921–1925 (1999).
12. W. Zhai, M. Slatkin, R. Nielsen, *J. Mol. Evol.* **65**, 340–348 (2007).
13. S. L. Kosakovsky Pond, A. F. Poon, A. J. Leigh Brown, S. D. Frost, *Mol. Biol. Evol.* **25**, 1809–1824 (2008).
14. D. C. Wiley, I. A. Wilson, J. J. Skehel, *Nature* **289**, 373–378 (1981).
15. I. A. Wilson, N. J. Cox, *Annu. Rev. Immunol.* **8**, 737–787 (1990).
16. D. J. Smith *et al.*, *Science* **305**, 371–376 (2004).
17. See supplementary materials on *Science* Online.
18. E. de Wit *et al.*, *J. Gen. Virol.* **88**, 1281–1287 (2007).
19. J. J. Skehel, D. C. Wiley, *Annu. Rev. Biochem.* **69**, 531–569 (2000).
20. J. J. Skehel *et al.*, *Proc. Natl. Acad. Sci. U.S.A.* **81**, 1779–1783 (1984).
21. Y. Abe *et al.*, *J. Virol.* **78**, 9605–9611 (2004).
22. B. P. Blackburne, A. J. Hay, R. A. Goldstein, *PLOS Pathog.* **4**, e1000058 (2008).

Acknowledgments: We thank M. Aban, G. van Amerongen, C. Baas, R. van Beek, M. de Graaf, S. Herfst, S. James, M. Linster, K. Sutherland-Cash, and C. Whittleston for excellent technical assistance and discussions. D.F.B. and D.J.S. acknowledge the use of the CamGrid distributed computing resource. Supported by an NWO VICI grant, National Institute of Allergy and Infectious Diseases contract HHSN266200700010C, NIH Director's Pioneer Award DP1-OD000490-01, European Union FP7 program EMPERIE (223498), European Union FP7 program ANTIGONE (278976), and program grant P0050/2008 from the Human Frontier Science Program. The Melbourne WHO Collaborating Centre for Reference and Research on Influenza is supported by the Australian Government Department of Health and Aging. A.D.M.E.O. (on behalf of Viroclinics Biosciences B.V.) has advisory affiliations with GSK, Novartis, and Roche. A.D.M.E.O. and G.F.R. are consultants for Viroclinics Biosciences BV. A/H3N2 virus sequences were previously published by Smith *et al*. (*16*). The sequences of the influenza A/H1N1 and B viruses used in this study are available from the GISAID EpiFlu Database (www.gisaid.org) and are listed in table S6.

Supplementary Materials

www.sciencemag.org/content/342/6161/976/suppl/DC1
Materials and Methods
Figs. S1 to S13
Tables S1 to S6
References (*23*–*29*)

15 August 2013; accepted 17 October 2013
10.1126/science.1244730

Yeast Reveal a "Druggable" Rsp5/Nedd4 Network that Ameliorates α-Synuclein Toxicity in Neurons

Daniel F. Tardiff,[1] Nathan T. Jui,[2] Vikram Khurana,[1,3] Mitali A. Tambe,[4] Michelle L. Thompson,[5]* Chee Yeun Chung,[1] Hari B. Kamadurai,[6] Hyoung Tae Kim,[7] Alex K. Lancaster,[1]† Kim A. Caldwell,[5] Guy A. Caldwell,[5] Jean-Christophe Rochet,[4] Stephen L. Buchwald,[2] Susan Lindquist[1,8]‡

α-Synuclein (α-syn) is a small lipid-binding protein implicated in several neurodegenerative diseases, including Parkinson's disease, whose pathobiology is conserved from yeast to man. There are no therapies targeting these underlying cellular pathologies, or indeed those of any major neurodegenerative disease. Using unbiased phenotypic screens as an alternative to target-based approaches, we discovered an *N*-aryl benzimidazole (NAB) that strongly and selectively protected diverse cell types from α-syn toxicity. Three chemical genetic screens in wild-type yeast cells established that NAB promoted endosomal transport events dependent on the E3 ubiquitin ligase Rsp5/Nedd4. These same steps were perturbed by α-syn itself. Thus, NAB identifies a druggable node in the biology of α-syn that can correct multiple aspects of its underlying pathology, including dysfunctional endosomal and endoplasmic reticulum–to-Golgi vesicle trafficking.

Phenotypic cell–based drug screens are a powerful yet underused approach to identify lead compounds and probe the underlying cellular pathologies that cause human disease (*1*). Such unbiased screens may be particularly helpful for neurodegenerative diseases (NDs), such as Parkinson's disease (PD) and Alzheimer's disease (AD), for which the molecular underpinnings of disease remain unclear. However, establishing robust neuronal phenotypes amenable to high-throughput screening and subsequent target identification remains a challenge. To bridge this gap, we exploited yeast cells that express ND-causing proteins to recapitulate salient cellular pathologies. α-Synuclein (α-syn), for example, causes derangements in vesicle trafficking, metal ion homeostasis, and mitochondrial function that are associated with α–synucleinopathies, such as PD (*2*). The resulting growth inhibition greatly facilitates robust high-throughput screening.

We recently screened ~190,000 compounds for their ability to restore the growth of cells

expressing toxic levels of TDP-43 (*3*), a protein associated with diverse NDs. A weak hit from that screen, an N-aryl benzimidazole (NAB) (Fig. 1A), proved more potent and effective against α-syn toxicity (Fig. 1B). NAB reversed diverse phenotypes caused by α-syn (*4*–*7*), including the accumulation of vesicular α-syn foci (Fig. 1C) (*8*, *9*), the generation of reactive oxygen species (Fig. 1D), the block of endoplasmic reticulum (ER)–Golgi trafficking (Fig. 1E), and the nitration of proteins (*6*). The toxicity of α-syn is extremely dependent on expression levels (*7*, *10*); however, NAB did not reduce α-syn accumulation (Fig. 1E).

[1]Whitehead Institute for Biomedical Research (WIBR), Cambridge, MA 02142, USA. [2]Department of Chemistry, Massachusetts Institute of Technology (MIT), Cambridge, MA 02139, USA. [3]Department of Neurology, Massachusetts General Hospital and Harvard Medical School, Boston, MA 02114,USA. [4]Department of Medicinal Chemistry and Molecular Pharmacology, Purdue University, West Lafayette, IN 47907, USA. [5]Department of Biological Sciences, University of Alabama, Tuscaloosa, AL 35487, USA. [6]Department of Structural Biology, St. Jude Children's Research Hospital, Memphis, TN 38018, USA. [7]Department of Cell Biology, Harvard Medical School, Boston, MA 02115, USA. [8]Howard Hughes Medical Institute (HHMI), Department of Biology, MIT, Cambridge, MA 02139, USA.

*Present address: Department of Pharmacology, University of Arizona, 1501 North Campbell Avenue, Tucson, AZ 85716, USA.

†Present address: Department of Pathology, Beth Israel Deaconess Medical Center, 330 Brookline Avenue, Boston, MA 02215, USA; and Center for Biomedical Informatics, Harvard Medical School, 10 Shattuck Street, Boston, MA 02115, USA.

‡Corresponding author. E-mail: lindquist_admin@wi.mit.edu

We next asked whether the protective activity of NAB was conserved in neurons. First, we tested a nematode model in which PD-relevant dopaminergic (DA) neurons degenerate in an age-dependent manner in response to human α-syn expression (*5*). Second, we tested rat primary neuronal cultures in which adenoviral expression of a familial α-syn mutation (A53T) causes selective loss of DA neurons: Tyrosine-hydroxylase (TH)–positive cells are lost, and neuronal processes retract (*4*, *5*). Third, we tested cortical neurons differentiated from PD-patient induced pluripotent stem cells (iPSCs) carrying either the A53T α-syn mutation or an α-syn triplication, both of which caused protein trafficking defects and nitrosative stress (*6*). In each case, NAB reversed α-syn toxicity or pathology, suggesting that the compound's target and mechanisms of action (MOA) were conserved from yeast to human cells (Fig. 1, F and G, and fig. S1) (*6*).

Yeast screens can reveal the target space for small molecules that suppress growth by identifying genetic alterations that restore it (*11*). At concentrations higher than those that rescued α-syn toxicity, NAB inhibited the growth of wild-type (WT) cells. To test whether α-syn rescue and growth inhibition had related MOA, we synthesized 29 NAB analogs (fig. S2). Compounds inactive in rescuing α-syn did not reverse α-syn foci formation or rescue ER-to-Golgi trafficking (fig. S3). Compounds that potently rescued α-syn also more potently inhibited growth in WT cells (Fig. 2A, fig. S2, and supplementary text). This allowed us to use genetic screens in WT cells to investigate NAB's MOA. Although NAB inhibited growth, cells retained full viability (Fig. 2B).

Using our most potent analog, NAB2, we selected for genetic alterations that allowed growth at high concentrations. We used three approaches: (i) a library of overexpression strains covering most genes in the yeast genome (~5800 genes), (ii) a library of ~300,000 random transposon-insertions (*12*), and (iii) spontaneous genomic point mutations arising from ~2 million cells (fig. S4). A small number of hits were recovered and formed a highly connected network of functionally related genes (Fig. 2C). These were an E3 ubiquitin ligase that promotes endosomal transport (*RSP5*), endocytic proteins (*SLA1*, *VRP1*), a multivesicular body sorting deubiquitinase (*DOA4*), an Rsp5 adaptor (*BUL1*), two proteins that can deubiquitinate Rsp5 substrates (*UBP7* and *UBP11*), known and potential Rsp5 substrates (*BAP2*, *BAP3*, and *MMP1*), and *VPS23*, which directs Rsp5 substrates for degradation in the vacuole (Fig. 2C). Analogs ineffective against α-syn did not exhibit dosage sensitivity with NAB network genes (fig. S5), supporting a related MOA between α-syn rescue and growth inhibition of WT cells.

The network topology of screen hits, and the nature of their altered dosage-sensitivity to NAB2 (figs. S6 to S8), suggested that NAB acts on Rsp5 to promote ubiquitin-mediated endosomal transport. With the exception of *RSP5*, which is es-

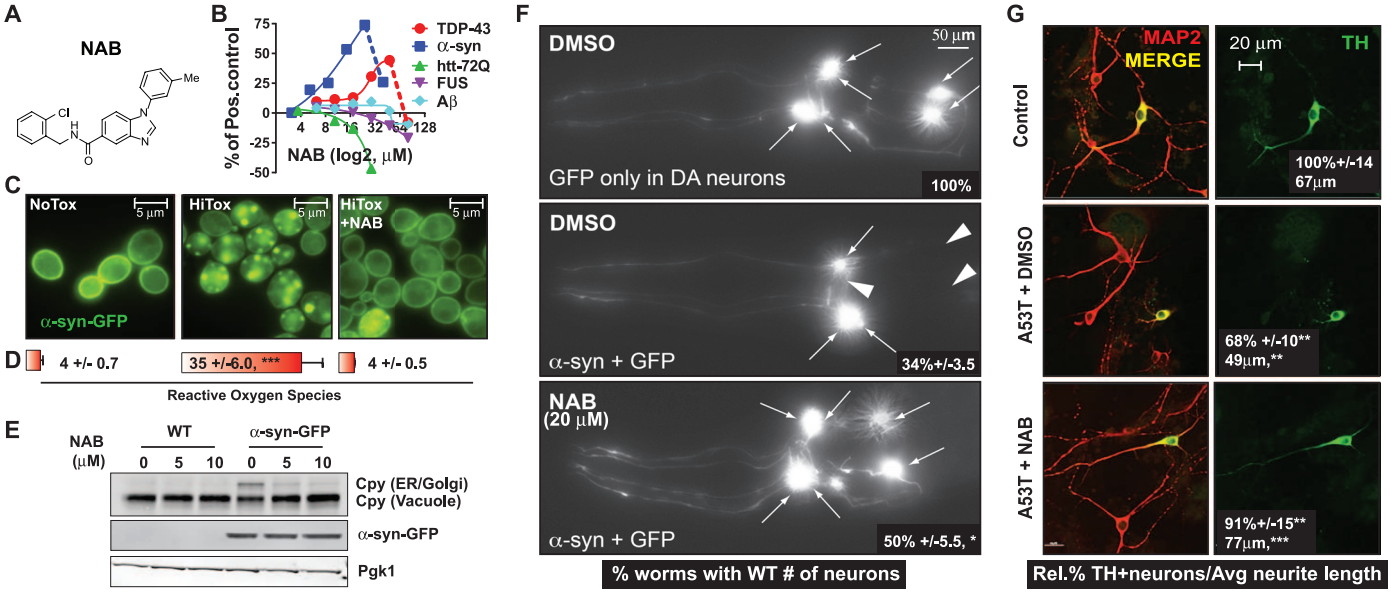

Fig. 1. NAB protects yeast and neurons from α-syn toxicity. (**A**) NAB structure. (**B**) Dose-response curves for NAB in yeast proteinopathy models. (**C**) α-syn–GFP localization in NoTox, HiTox, and HiTox/10 μM NAB. (**D**) Percent of reactive oxygen species–positive cells under same conditions as (C). Values are mean ± SD; $n = 3$ independent trials. (**E**) Immunoblot of Cpy showing ER-Golgi trafficking defect and α-syn protein levels in WT and HiTox cells treated with NAB. (**F**) Fluorescence microscopy of the six anterior DA neurons in representative *C. elegans* expressing either GFP or human α-syn and GFP after treatment with dimethyl sulfoxide (DMSO) or NAB. Arrows indicate intact DA neuron cell bodies and arrowheads indicate regions where these cells have degenerated. Inlaid values reflect mean ± SD; $n = 3$ independent trials. (**G**) Representative images of DA-enriched cultures established from embryonic rat midbrains. Control, untransduced; A53T, transduced with A53T α-syn virus; red, MAP2 (neuronal tubulin); green, TH-positive neurons. Inlaid values reflect mean with control set to 100% and ± SD; $n = 3$ independent trials for percent TH-positive neurons and mean ± SEM, $n = \sim 75$ neurons for neurite length. For all data: $^*P < 0.05$; $^{**}P < 0.01$; $^{***}P < 0.001$ using one-way analysis of variance (ANOVA) and a Tukey's test.

sential, every other gene in our network could be deleted. But no deletion (including a double deletion of *UBP7* and *UBP11*) conferred more than partial resistance to NAB2. Thus, although these other proteins are involved in NAB2 activity, they cannot themselves be its target. Indeed, the effects of altering *RSP5* gene dosage indicate that it is the central node: Increased *RSP5* dosage increased sensitivity to NAB2, and decreased *RSP5* dosage decreased sensitivity to NAB2 (Fig. 2D). Furthermore, in otherwise isogenic cells a single amino acid substitution in the ~1000-amino-acid protein ($rsp5_{G747E}$) conferred resistance to NAB2 (Fig. 2D and fig. S7).

Rsp5 is the single yeast member of the highly conserved mammalian family of HECT domain Nedd4 E3 ligases. These proteins catalyze K63 linkages of ubiquitin to diverse membrane proteins and thereby regulate endosomal trafficking, not proteasomal degradation (*13*, *14*). HECT domain ubiquitin ligases contain multiple protein-protein interaction domains that bind diverse adaptor proteins and substrates. Calcium, lipid binding, and autoinhibitory conformations regulate substrate specificity and endosomal transport from either the plasma membrane or Golgi to the vacuole/lysosome. Most aspects of these complex modes of Rsp5 regulation have not been recapitulated in vitro.

Therefore, to further investigate NAB2 activities we monitored, in WT cells, its effects on three proteins whose trafficking depends on Rsp5: Mup1 (*15*), Sna3 (*16*), and Bap2 (*17*). NAB2 (i) promoted the Rsp5-dependent endocytosis and vacuolar delivery of the methionine permease, Mup1 (Fig. 2E and fig. S9); (ii) promoted the Rsp5-dependent Golgi-to-vacuole trafficking of the adaptor protein Sna3 (Fig. 2F and fig. S9); and (iii) promoted the Rsp5-dependent degradation of the leucine permease Bap2 (fig. S10). (This affected leucine-dependent growth, explaining its recovery in our overexpression screen.)

We further established the relevance of the NAB/Rsp5 network by genetically altering screen hits in the context of α-syn. Indeed, most but not all genetic manipulations that antagonized NAB2 activities in WT cells antagonized its activities against α-syn toxicity. For example, deleting Δ*sla1* and Δ*vps23*, or overexpressing the deubiquitinases *UBP7* and *UBP11*, all partially compromised the ability of NAB2 to rescue α-syn toxicity (Fig. 3A and fig. S11). Deleting Δ*ubp7* and Δ*ubp11*, either singly or in combination, had no effect on NAB2's rescue of α-syn toxicity (fig. S11).

The spontaneous point mutation recovered in our screen, $rsp5_{G747E}$, which compromised Rsp5 activity (Fig. 2, E and F, and fig. S7) and conferred resistance to NAB2 in WT cells, shifted the dose of NAB2 required for α-syn rescue in a complementary fashion (Fig. 3A). Consistent with this, $rsp5_{G747E}$ prevented NAB2 from fully reverting the formation of α-syn foci (Fig. 3B) and from restoring ER-to-Golgi trafficking (Fig. 3C)

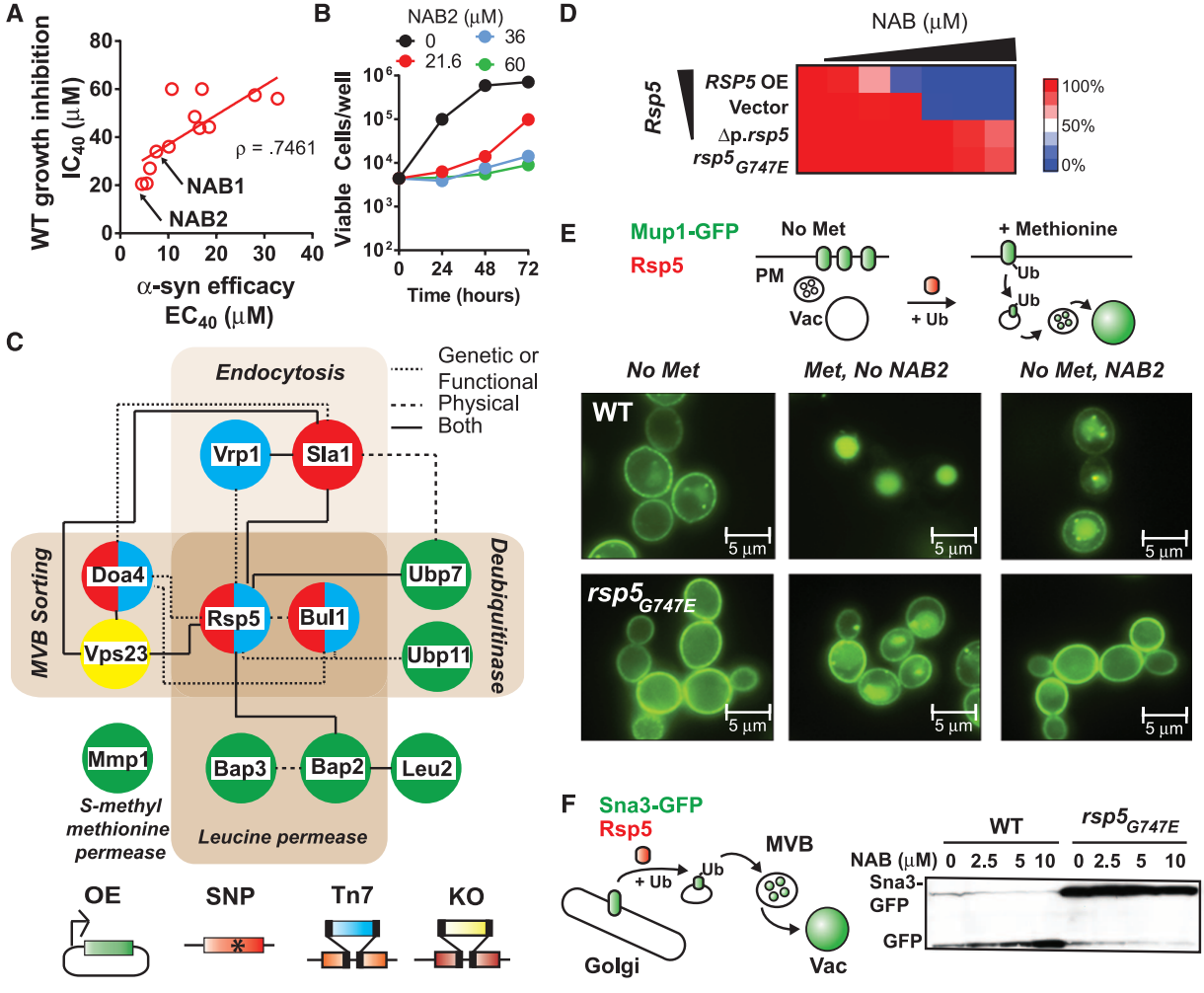

Fig. 2. Chemical genetic screens of NAB2 reveal a network centered on the E3 ligase, Rsp5. (**A**) Efficacy (EC_{40}) in α-syn cells versus growth inhibition (IC_{40}) in WT cells for active analogs. NAB1 is the screen hit, and NAB2 is the most potent analog. (**B**) Viable cells recovered after prolonged NAB2 treatment. (**C**) NAB2 interaction network. Node color reflects screen of origin indicated below. Edges are interactions (legend, top right) according to String database and literature. *VPS23* was deleted after identification of other hits. (**D**) Heat map of *RSP5* variant cell growth in response to increasing NAB2 compared with untreated cells. Mutants include $rsp5_{G747E}$ and the hypomorphic allele, Δ*p.rsp5*. (**E**) (Top) Methionine- and Rsp5-dependent Mup1-GFP endocytosis. (Bottom) Mup1-GFP localization in WT and $rsp5_{G747E}$ strains under indicated conditions. (**F**) (Left) Schematic of Sna3-GFP endosomal trafficking to the vacuole, where GFP is cleaved. (Right) Immunoblot analysis of Sna3-GFP in WT and $rsp5_{G747E}$ cells treated with NAB2.

phenotypes. Together, these analyses established Rsp5 as the central node and only potential protein target within the NAB network.

Rsp5's importance in modifying α-syn toxicity was highlighted by integrating the NAB/Rsp5 and α-syn genetic networks (table S3) (*4*, *18*). These interactions connected our NAB network to nearly 30% of the previously established genetic modifiers of α-syn toxicity, including those that function in Golgi/vesicular transport, endosomal transport, lipid metabolism, protein catabolism, and tubulin assembly (Fig. 3D and fig. S12).

Next, we tested α-syn's effect on Mup1–green fluorescent protein (GFP) and Sna3-GFP trafficking. Indeed, α-syn expression impeded both the methionine-induced transport of Mup1-GFP from the plasma membrane to the vacuole (Fig. 4A) and the constitutive trafficking of Sna3-

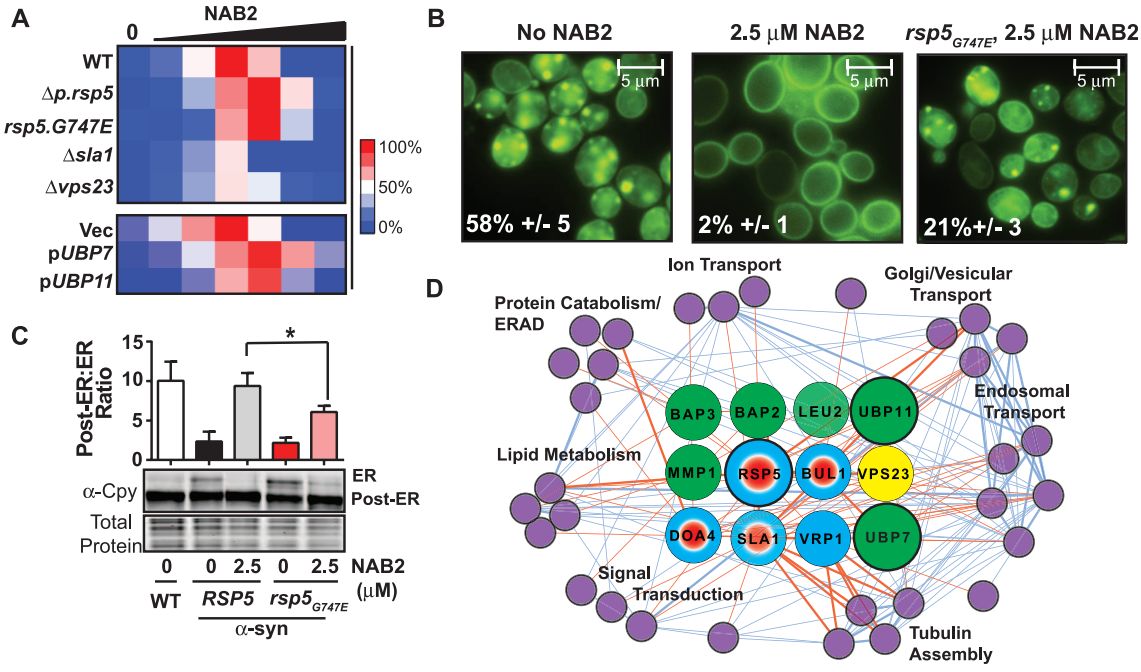

Fig. 3. NAB/Rsp5 network directly affects rescue of α-syn toxicity. (**A**) Heat map of NAB2 dose-response in WT and modified α-syn strains. Rescue is relative to EC_{100} for NAB2 in WT α-syn cells. (**B**) α-syn–GFP localization in WT or $rsp5_{G747E}$ α-syn cells under indicated conditions. Inlaid values indicate percent of cells with large α-syn foci (mean ± SD, $n = 3$ independent trials). (**C**) Immunoblot of Cpy trafficking defect α-syn cells with DMSO or NAB2. *$P < 0.05$ using one-way ANOVA. (**D**) Interaction network of α-syn and NAB2 genetic modifiers. α-syn nodes, purple; NAB2 nodes are color-coded according to screen of origin (Fig. 2C). *RSP5*, *UBP7*, and *UBP11* are larger because they both suppress NAB2 growth inhibition and enhance α-syn toxicity (*4*). Edges between nodes depict physical or genetic interactions. Thicker lines indicate both genetic and physical interactions. Red edges link node interactions between α-syn and NAB2 networks. Remaining α-syn edges are blue.

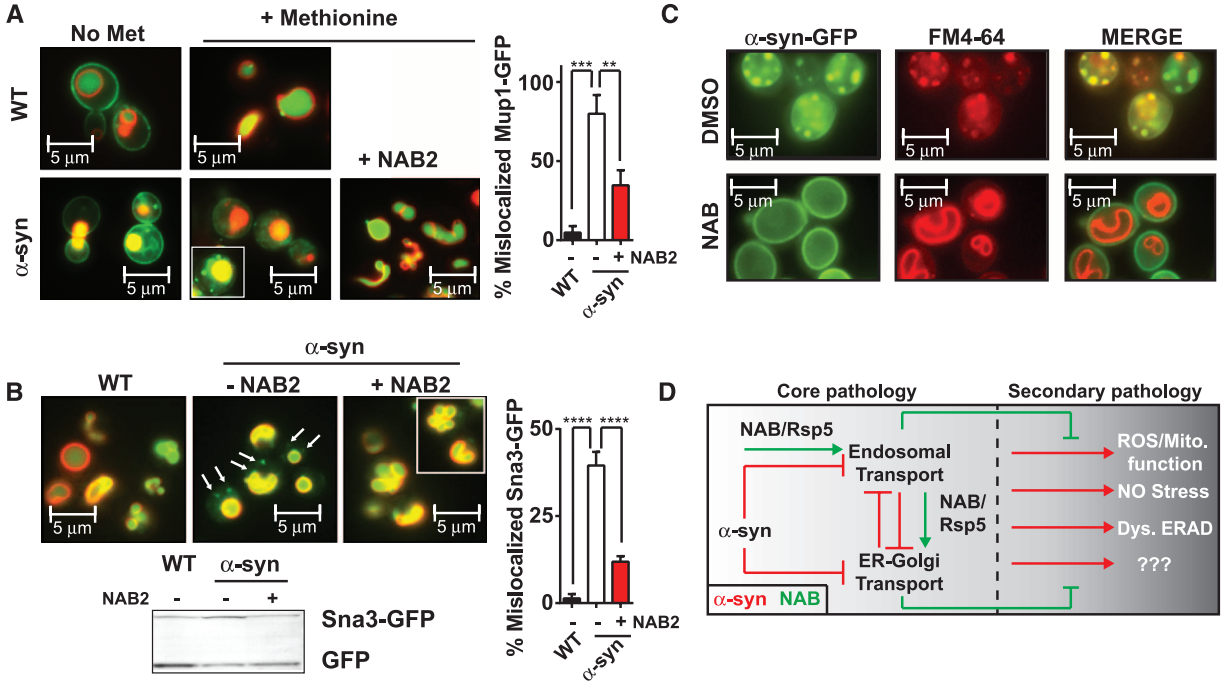

Fig. 4. NAB2 directly antagonizes α-syn–induced endosomal defects. (**A**) Methionine-stimulated Mup1-GFP endocytosis in WT or untagged α-syn strains with DMSO or NAB2. Pulse-labeling cells with FM4-64 during the first hour of α-syn expression marked the vacuole. (**B**) Effects of α-syn on Sna3-GFP localization. Immunoblot shows Sna3-GFP cleavage in response to α-syn and NAB. FM4-64 labeling is as in (A). Arrows indicate stalled endosomal vesicles containing Sna3-GFP. (**C**) Pulse-labeling of FM4-64 of α-syn cells after 4 hours of expression in the presence or absence of NAB2. (**D**) Schematic of NAB2 mechanism in antagonizing core and secondary α-syn pathologies.

GFP from the Golgi and the vacuole (Fig. 4B). Further, in the presence of α-syn, NAB2 restored trafficking of both substrates (Fig. 4, A and B).

In addition to specific substrates, bulk endosomal transport from the plasma membrane to the vacuole was perturbed by α-syn (Fig. 4C) (*7*–*9*, *19*). When FM4-64 was used to pulse-label the endosomal pathway, after prolonged α-syn expression the dye strongly colocalized with α-syn inclusions and failed to reach the vacuole (Fig. 4C). NAB2 fully restored endocytosis and concomitantly reduced α-syn inclusions (Fig. 4C, bottom). Thus, the ability of NAB to promote Rsp5-dependent processes directly restored diverse cellular pathologies caused by α-syn, including both ER-to-Golgi and endosomal trafficking (Fig. 4D and fig. S8).

Rsp5/Nedd4 can ubiquitinate α-syn, and Nedd4 localizes to Lewy Bodies in brain samples from PD patients (*20*). However, α-syn levels were not altered by NAB2 in vivo (Fig. 1E). And when tested in vitro, NAB2 did not affect the ubiquitination of α-syn and Sna3 by Rsp5 (fig. S13). As noted, however, most of the complexities of Rsp5 in vivo activities have yet to be recapitulated in vitro. Thus, NAB2 exemplifies the ability of unbiased in vivo phenotypic screens to uncover chemical probes that cannot be discovered through simple target-based in vitro approaches. Likewise, NAB2 chemical genetics identify a deeply rooted biological node, Rsp5, that had not been identified in previous overexpression or deletion screens. Despite their central role in protein homeostasis and several human diseases, to date E3 ubiquitin ligases are virtually untouched by biological probes, let alone therapeutics.

The vesicular trafficking processes perturbed by α-syn and promoted by NAB are fundamental to all eukaryotic cells yet are particularly important to neurons that rely heavily on efficient synaptic vesicle dynamics and regulated neurotransmitter release. Indeed, dysfunctional endosomal transport is emerging as a contributing factor in α-syn pathology in human neurons. Altered cell biology, post mortem pathology, and human genetic risk factors all implicate altered vesicular trafficking (*4*, *7*–*9*, *19*, *21*–*25*). The ability of NAB to promote endosomal trafficking through Rsp5/Nedd4 and thus "reset" vesicle trafficking homeostasis, in turn, rescued several other, seemingly disparate, α-syn phenotypes. Identifying such deeply rooted pathways that ramify to affect multiple aspects of protein-folding pathology may be critical for developing disease-modifying therapies.

References and Notes

1. D. C. Swinney, J. Anthony, *Nat. Rev. Drug Discov.* **10**, 507–519 (2011).
2. V. Khurana, S. Lindquist, *Nat. Rev. Neurosci.* **11**, 436–449 (2010).
3. D. F. Tardiff, M. L. Tucci, K. A. Caldwell, G. A. Caldwell, S. Lindquist, *J. Biol. Chem.* **287**, 4107–4120 (2012).
4. A. A. Cooper *et al.*, *Science* **313**, 324–328 (2006).
5. L. J. Su *et al.*, *Dis. Model. Mech.* **3**, 194–208 (2010).
6. C. Y. Chung *et al.*, *Science* **342**, XXX (2013).
7. T. F. Outeiro, S. Lindquist, *Science* **302**, 1772–1775 (2003).
8. A. D. Gitler *et al.*, *Proc. Natl. Acad. Sci. U.S.A.* **105**, 145–150 (2008).
9. J. H. Soper, V. Kehm, C. G. Burd, V. A. Bankaitis, V. M. Lee, *J. Mol. Neurosci.* **43**, 391–405 (2011).
10. A. B. Singleton *et al.*, *Science* **302**, 841 (2003).
11. A. M. Smith, R. Ammar, C. Nislow, G. Giaever, *Pharmacol. Ther.* **127**, 156–164 (2010).
12. A. Kumar, *Methods Mol. Biol.* **416**, 117–129 (2008).
13. D. Rotin, S. Kumar, *Nat. Rev. Mol. Cell Biol.* **10**, 398–409 (2009).
14. E. Lauwers, Z. Erpapazoglou, R. Haguenauer-Tsapis, B. André, *Trends Cell Biol.* **20**, 196–204 (2010).
15. A. Menant, R. Barbey, D. Thomas, *EMBO J.* **25**, 4436–4447 (2006).
16. C. MacDonald, D. K. Stringer, R. C. Piper, *Traffic* **13**, 586–598 (2012).
17. F. Omura, Y. Kodama, T. Ashikari, *FEMS Microbiol. Lett.* **194**, 207–214 (2001).
18. E. Yeger-Lotem *et al.*, *Nat. Genet.* **41**, 316–323 (2009).
19. V. Sancenon *et al.*, *Hum. Mol. Genet.* **21**, 2432–2449 (2012).
20. G. K. Tofaris *et al.*, *Proc. Natl. Acad. Sci. U.S.A.* **108**, 17004–17009 (2011).
21. G. Esposito, F. Ana Clara, P. Verstreken, *Dev. Neurobiol.* **72**, 134–144 (2012).
22. D. A. MacLeod *et al.*, *Neuron* **77**, 425–439 (2013).
23. C. Vilariño-Güell *et al.*, *Am. J. Hum. Genet.* **89**, 162–167 (2011).
24. A. Zimprich *et al.*, *Am. J. Hum. Genet.* **89**, 168–175 (2011).
25. P. Zabrocki *et al.*, *Biochim. Biophys. Acta* **1783**, 1767–1780 (2008).

Acknowledgments: We thank A. Kumar for providing the plasmid Tn7 library; B. Wendland and L. Hicke for the Rsp5 antibody; the WIBR Genome Technology Core for Illumina Sequencing; B. Schulman (B. Schulman and H.B.K. were funded by NIH grant 5R01GM069530) and A. Goldberg for help with in vitro ubiquitination assays; T. DiCesare for graphics support; and members of the Lindquist Lab for helpful comments on the manuscript. S.L. is an investigator for HHMI. D.F.T. was funded by a National Research Service Award (NRSA) fellowship F32NS061419 and research supported by the JPB Foundation (D.F.T. and S.L.), the Eleanor Schwartz Charitable Foundation, and an HHMI Collaborative Innovation Award (D.F.T., V.K., C.Y.C., and S.L.; G.A.C., K.A.C., and M.L.T.; and J.-C.R. and M.A.T.). N.T.J. was funded by a NRSA fellowship (F32GM099817), and N.T.J. and S.L.B. were funded by NIH grant GM58160. H.T.K. was funded by the Bachmann-Strauss Dystonia & Parkinson Foundation. Genome sequencing data are deposited in the National Center for Biotechnology Information under BioProject accession number PRJNA222476. WIBR and MIT have filed a patent application, on which D.F.T., N.T.J., S.L.B., and S.L. are inventors, relating to use of compounds described here in treatment of neurodegenerative diseases. In addition, S.L. is an inventor on patents and patent applications filed by the University of Chicago relating to methods of screening for compounds that decrease α-syn–associated toxicity using yeast that express α-syn. All the yeast plasmids and strains and NAB are available under a Uniform Biological Material Transfer Agreement from the Whitehead Institute.

Supplementary Materials

www.sciencemag.org/content/342/6161/979/suppl/DC1
Materials and Methods
Supplementary Text
Figs. S1 to S13
Tables S1 to S3
References (*26*–*50*)

29 August 2013; accepted 16 October 2013
Published online 24 October 2013;
10.1126/science.1245321

Identification and Rescue of α-Synuclein Toxicity in Parkinson Patient–Derived Neurons

Chee Yeun Chung,[1]* Vikram Khurana,[1,2]* Pavan K. Auluck,[1,3] Daniel F. Tardiff,[1] Joseph R. Mazzulli,[2] Frank Soldner,[1] Valeriya Baru,[1,4] Yali Lou,[1,4] Yelena Freyzon,[1] Sukhee Cho,[5] Alison E. Mungenast,[5] Julien Muffat,[1] Maisam Mitalipova,[1] Michael D. Pluth,[6] Nathan T. Jui,[6] Birgitt Schüle,[7] Stephen J. Lippard,[6] Li-Huei Tsai,[4,5] Dimitri Krainc,[2] Stephen L. Buchwald,[6] Rudolf Jaenisch,[1,8] Susan Lindquist[1,4,8]†

The induced pluripotent stem (iPS) cell field holds promise for in vitro disease modeling. However, identifying innate cellular pathologies, particularly for age-related neurodegenerative diseases, has been challenging. Here, we exploited mutation correction of iPS cells and conserved proteotoxic mechanisms from yeast to humans to discover and reverse phenotypic responses to α-synuclein (αsyn), a key protein involved in Parkinson's disease (PD). We generated cortical neurons from iPS cells of patients harboring αsyn mutations, who are at high risk of developing PD dementia. Genetic modifiers from unbiased screens in a yeast model of αsyn toxicity led to identification of early pathogenic phenotypes in patient neurons. These included nitrosative stress, accumulation of endoplasmic reticulum (ER)–associated degradation substrates, and ER stress. A small molecule identified in a yeast screen (NAB2), and the ubiquitin ligase Nedd4 it affects, reversed pathologic phenotypes in these neurons.

Neurodegenerative dementias are devastating and incurable diseases for which we need tractable cellular models to investigate pathologies and discover therapeutics. Parkinson's disease dementia (PDD), a debilitating nonmotor manifestation of Parkinson's disease (PD), affects as many as 80% of patients (*1*). The best pathological correlate of PDD is neuron loss and pathological aggregation of α-synuclein (αsyn) within deep layers of the cerebral cortex (*1*). Contursi kindred patients, who harbor an autosomal dominant and highly penetrant $Ala^{53}\rightarrow Thr^{53}$ (A53T) mutation in αsyn, manifest prominent PD and dementia (*2*, *3*). Induced pluripotent stem (iPS) cells from a female member of this kindred (table S1) have recently been mutation-corrected to control for genetic background effects (*4*). To establish a model for cortical synucleinopathy, we differentiated